Supplementary Fig. 1

HVCN1 expression in B-cell tumors and anti-HVCN1 antibody specificity.

(a) Immunohistochemical staining of diffuse large B-cell lymphoma (DLBCL) tumors with anti-HVCN1 anti-serum showing membranous (left panel) and Golgi-like staining (right panel); the causes and consequences of the apparently aberrant subcellular localization of HVCN1 in the Golgi in some DLBCL are not known. In cases of mantle-cell lymphoma, high HVCN1 expression was seen in peripheral blood cells (which are mainly in G_0) but not in proliferating cells within the lymph node (not shown). Suenaga et al. also found HVCN1 expression to associate with reduced proliferation in B cells in HVCN1 transgenic mice[54], likely due to aberrant expression in pre-B/immature B cells. However, they did not investigate the effect of HVCN1 lack of expression in mature, peripheral B cells, which normally express it, upon BCR stimulation.

(b) Immunoblot of chronic lymphocytic leukemia (CLL) peripheral cells probed with anti-HVCN1 anti-serum. Numbers indicate different patients' samples. IRM2 mantle-cell lymphoma line was used as positive control. CLL peripheral cells exhibit a resting G_0 phenotype. Immunoblot analysis of normal and malignant B cells showed HVCN1 sometimes expressed as a doublet. The shorter protein isoform derives from a second initiation site downstream of the first ATG (not shown).

(c) Immunoblot analysis of LK35.2 cells ± over-expressed HVCN1, probed with anti-HVCN1 rabbit polyclonal anti-serum that recognizes a sequence in the N-terminus domain ($HVCN1_{26-46}$). EV indicates cells transduced with empty vector. Blot confirms anti-HVCN1 specificity, as LK35.2 cells do not express HVCN1 and do not have proton currents (Supplementary Fig. 3).

(d) Immunoblot of HEK293 cells transfected with HVCN1 and HVCN1 siRNAs to confirm specificity of the polyclonal anti-HVCN1 serum. SC=scramble siRNA; si1 and si2= siRNAs that recognize 2 different HVCN1 sequences. GFP (cotransfected with HVCN1 and siRNAs) indicates lanes loading control.

Capasso et al. supplementary Fig. 1

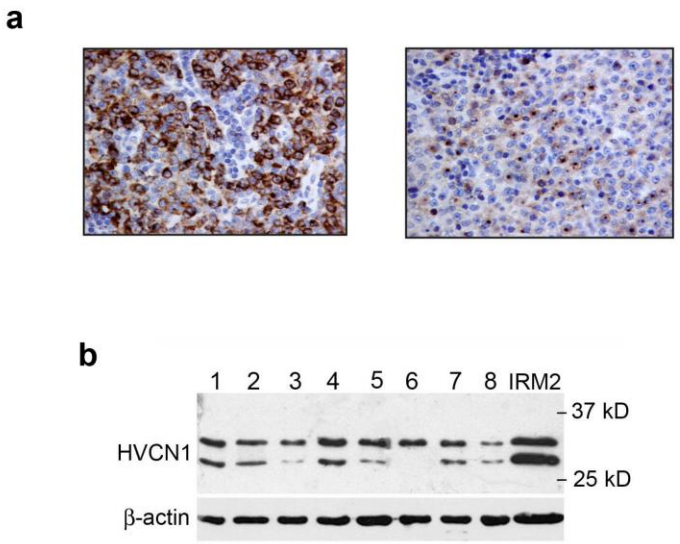

Supplementary Fig. 2

HVCN1 and IgM co-localization following BCR stimulation.

(a) Representative confocal image of a human primary B cell activated via IgM cross-linking, 5 min. after stimulation. IgM is in green, HVCN1 is in red. HLA-DR (blue) indicates the plasma membrane. DAPI staining indicates the nucleus.

(b) Electron microscopy image of co-internalized IgM and HVCN1 upon stimulation. BJAB cells over-expressing HA-tagged HVCN1 were stimulated with 20 μg/ml $F(ab')_2$ anti-IgM conjugated to 10 nm gold particles (medium arrows in right panel). HVCN1 was detected using anti-HA antibody followed by a 5 nm (small arrows in right panel) gold-conjugated secondary antibody. Cells were stimulated at 37° C for 60 min, then washed in ice-cold buffer and fixed.

(c) Immunoblot of fractions obtained by sucrose density centrifugation of protein lysates of a B-cell line, Namalwa, expressing exogenous myc-tagged HVCN1, before and after BCR stimulation. EEA-1 indicates early endosomes, Lamp-1 indicates late endosomes/lysosomes and HLA-DM indicates MIICs. Fractions 10-15 after BCR stimulation represent late endosomes/lysosomes (strong Lamp1 expression) containing now the majority of HVCN1. HLA-DM co-expression indicates these fractions represent MIICs. Blots are representative of 3 independent experiments.

(d) To assess whether PKC phosphorylation could affect BCR and HVCN1 co-internalization IgM cross-linking was performed in the presence of a PKC inhibitor. No impairment was observed in PKC-inhibited cells. Left panel, confocal image of a human peripheral blood B cell activated via IgM cross-linking in the presence of 3 μM of GFX (GF109203X), an inhibitor of PKC, 60 min. after stimulation. Right panel, quantification of co-localization between HVCN1 and IgM in the absence (▽) and presence of GFX (■). Pearson's coefficient gives a total value of co-localization, which can vary from 0 (= no co-localization) to 1 (= total co-localization). n=27 cells.

Capasso et al. supplementary Fig. 2

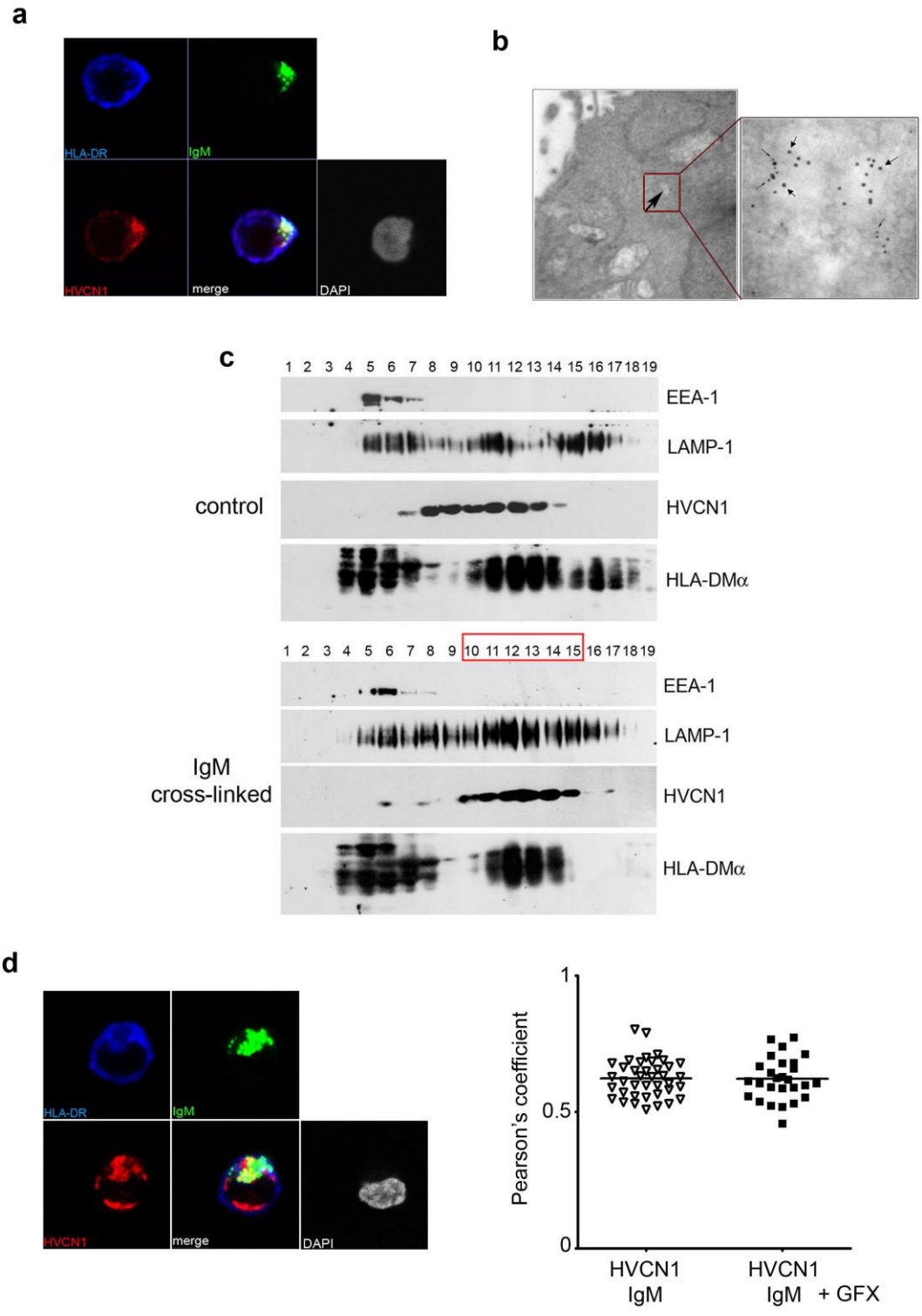

Supplementary Fig. 3

PKC-dependent HVCN1 phosphorylation after BCR stimulation and enhanced gating of proton currents upon PKC phosphorylation. ROS response in LK35.2 cells.

(a) Left panel, phosphorylation assay of LK35.2 HyHEL10 cells over-expressing HVCN1 showing its PKC-dependent phosphorylation upon activation. Cells were incubated with ^{32}P orthophosphate for 2h, then stimulated with 5 μM HEL for 15 min and lysed. Myc-tagged HVCN1 was immunoprecipitated with an anti-myc antibody and lysates run on a SDS-page for protein separation. After transfer to nitrocellulose membranes, membranes were exposed to X-ray film. Membranes were then immunoblotted with anti-myc to control efficiency of immunoprecipitation. The experiment was repeated in the absence and presence of 3 μM of the PKC inhibitor GFX (GF109203X). Right panel, densitometry analysis of ratios of radioactive signal vs. loading control. Values represent averages of 3 separate experiments. *$p < 0.05$ by Student's t test.
(b) IgM expression in LK35.2 cells transduced with empty vector (grey filled histogram) and HVCN1 (black empty histogram). Results are representative of at least 3 independent experiments.
(c) ROS assay on LK35.2 cells ± over-expressed HVCN1, stimulated with PMA or $F(ab')_2$ anti-IgM. Control cells are LK35.2 cells transduced with empty vector. The black triangles indicate ROS increase in WT splenic B cells for comparison. The experiment indicates ROS production is negligible in LK35.2 cells and was not increased by HVCN1 over-expression. Values represent average of 3 independent experiments. NADPH oxidase expression is low in LK35.2 cells (not shown).

Capasso et al. supplementary Fig. 3

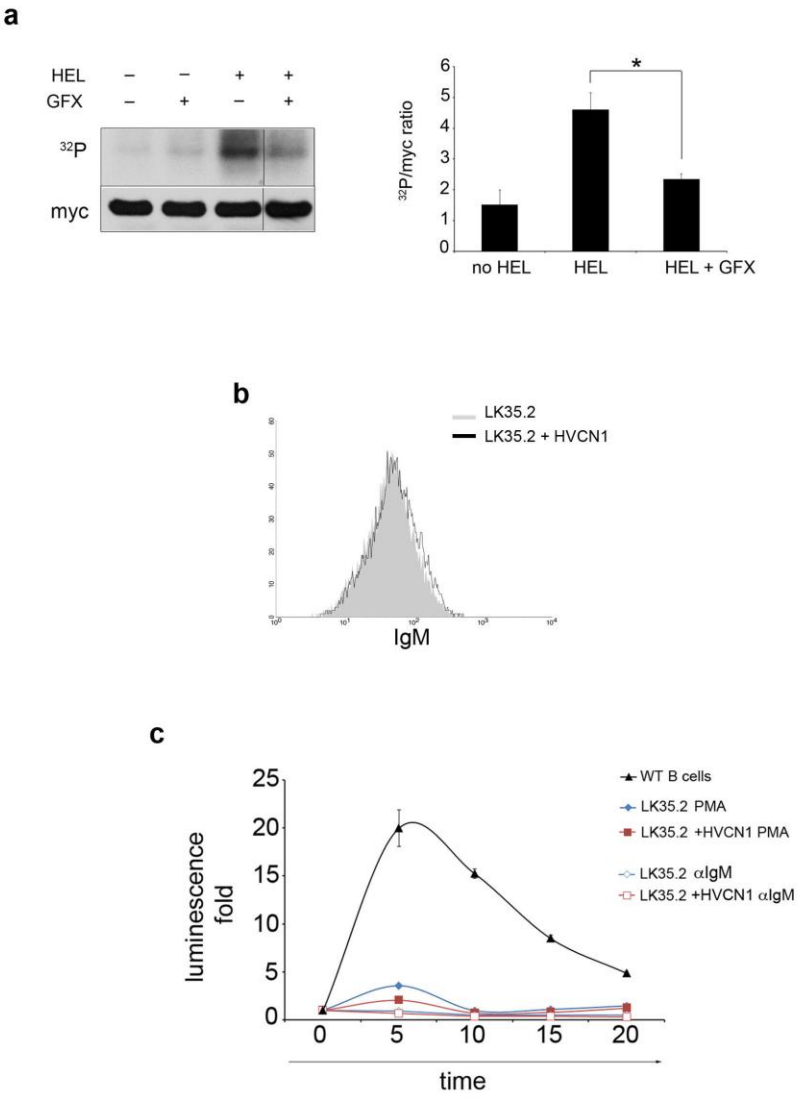

Supplementary Fig. 4

HVCN1 mRNA and protein expression in murine B cells.

(a) RT-PCR of HVCN1 and a housekeeping gene as control in wild-type cells (+/+), cells containing one allele with the gene-trap (+/gt) and cells containing both alleles with the gene-trap (gt/gt). The gene-trap is inserted in intron 3 of the HVCN1 gene, following exon 2, which contains the first translation initiation codon (not shown). HVCN1 primers were designed within exon 2 (forward primer) and exon 5 (reverse primer). Other reverse primers were designed on the other 4 coding exons and the 3' UTR. All showed absence of HVCN1 mRNA in cells derived from mice with the gene-trap on both alleles (not shown). The same gene-trap mouse line was employed elsewhere[25,26].

(b) Immunoblot analysis of protein lysates from wild-type and HVCN1-deficient splenic B cells, probed with the specific anti-HVCN1 anti-serum.

(c) Immunoblot of protein lysates of murine B cell subpopulations probed with anti-HVCN1.

Lanes represent: 1= pro-B ($CD19^+B220^{lo}IgM^-IgD^-CD25^-$), 2= pre-B ($CD19^+B220^{lo}IgM^-IgD^-CD25^+$), 3= immature B (($CD19^+B220^{lo}IgM^+IgD^-CD25^-$), 4= mature B ($CD19^+$ from lymph nodes), 5= splenic $B220^+$ cells from HVCN1-deficient mice, 6= splenic $B220^+$ cells from wild-type mice, 7= mature B ($CD19^+$ from lymph nodes), 8= B1a ($CD19^+IgM^+CD5^{lo}$) from the peritoneal cavity, 9= splenic marginal zone B ($CD19^+CD21^{hi}CD23^{lo}$). Only splenic B220+ and mature B cells from lymph nodes show clearly detectable HVCN1 expression.

(d) Proton currents are observed in WT B cells (left panel) but not in HVCN1-deficient B cells (right panel) voltage-clamped in perforated-patch configuration at pH 7. Left panel, a family of currents in a wild-type B cell during pulses from -20 mV to -10 mV through +60 mV in 10-mV increments. Right panel, a family of currents in an HVCN1-deficient B cell during pulses from -20 mV to -10 mV through +80 mV in 10-mV increments (n= 17, 5).

(e) HVCN1 (MGC15619) gene expression profile in human B-cell precursors from[27]. HSC= hematopoietic stem cells, E-B= early B cells, pro-B= pro-B cells, pre-B= pre-B cells, IMM-B= immature B cells. HVCN1 mRNA expression is absent in HSC but then gradually increases during B-cell differentiation.

Capasso et al. supplementary Fig. 4

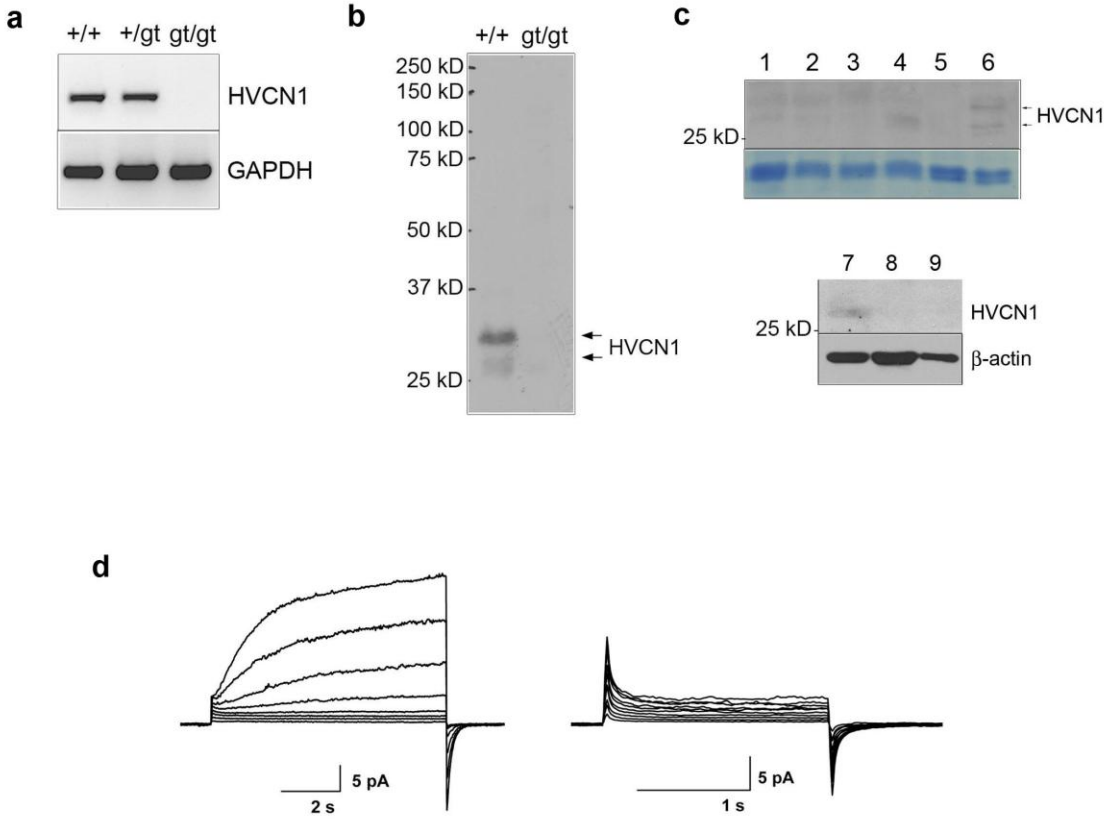

e

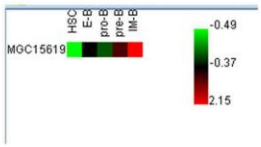

Gene expression (median)

GeneSymbol	HSC	E-B	pro-B	pre-B	IM-B
MGC15619	-0.49	-0.37	-0.41	0.40	2.15
Fold Change	0.712988148	0.772764112	0.754765299	1.321475795	4.441355335
Abs Fold Change	1.402547858	1.294055954	1.324915178	1.321475795	4.441355335

Supplementary Fig. 5

WT and HVCN1-deficient B-cell phenotype.

(a) Flow cytometry of splenic cells to identify B cell subsets: marginal zone B cells ($CD23^{lo}CD21^{hi}$) and follicular B cells ($CD23^{hi}CD21^{lo}$); B1a cells ($CD5^{lo}IgM^{+}$) and B2 cells ($CD5^{-}IgM^{+}$). Histograms on the right hand side indicate IgM expression for wild-type (grey filled histogram) and HVCN1-deficient (black empty histogram) splenocytes.
(b) B1a cells ($CD5^{lo}IgM^{+}$) and B1b and B2 cells ($CD5^{-}IgM^{+}$) from the peritoneal cavity (PC). Histograms indicate IgM expression of total peritoneal cells.
(c) flow cytometry of B cells from inguinal lymph nodes. Histograms indicate IgD (wild-type in red filled histogram, HVCN1-deficient in empty black histogram) and IgM expression in lymph node cells.
(d) staining of B-cell subsets in the bone marrow: pro-B and pre-B cells ($B220^{lo}IgM^{-}$), immature B ($B220^{lo}IgM^{+}$), transitional B ($B220^{lo\text{-}hi}IgM^{hi}$) and mature B ($B220^{hi}IgM^{+}$). Histograms indicate IgM expression in bone marrow cells. Numbers adjacent to boxed areas indicate percentages of cells in each gate. Results in all panels are representative of at least 5 wild-type and 5 HVCN1-deficient mice.
Overall, there was no consistent difference in proportions of any B-cell subpopulations in HVCN1-deficient mice compared to wild-type counterparts, nor in Ig surface expression.

Capasso et al. supplementary Fig. 5

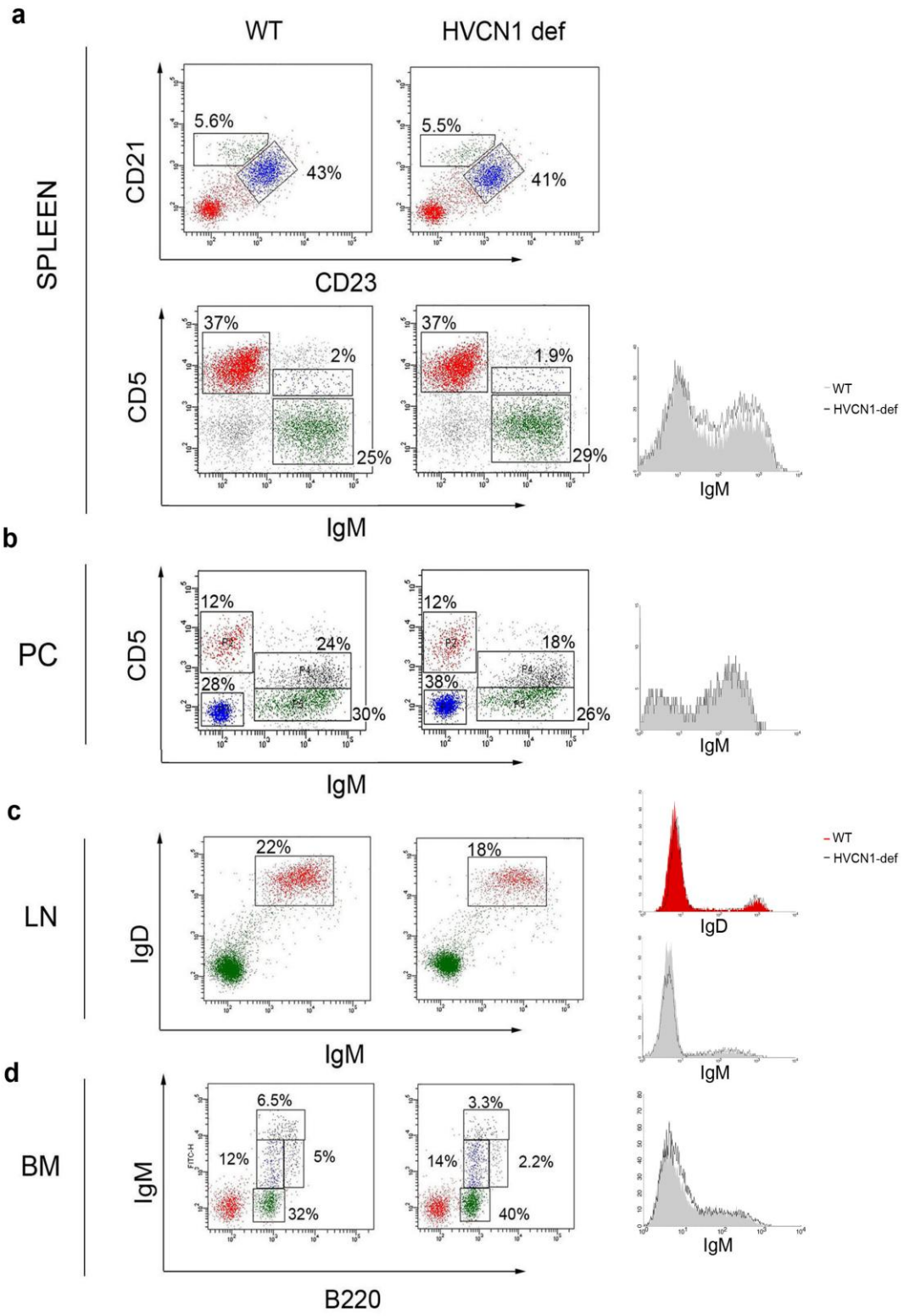

Supplementary Fig. 6

Effect of rotenone and DPI on basal ROS. Protein tyrosine phosphorylation in DPI-treated B cells and BCR-dependent ROS increase in the presence of sodium stibogluconate.

(a) Basal ROS in wild-type and HVCN1-deficient B cells measured with the intracellular dye DCFDA. UNT= untreated, ROTENONE= in the presence of 1 μM rotenone, DPI= in the presence of 10 μM DPI. Differences between wild-type and HVCN1-deficient cells treated with rotenone and DPI are not significant. n=3 mice.
(b) phospho-tyrosine blot of cells activated with 20 μg/ml $F(ab')_2$ anti-IgM in the presence of 5 μM DPI. Arrows indicate non specific bands. Blots represent 3 independent experiments.
(c) ROS increase in wild-type and HVCN1-deficient splenic B cells pretreated with 5 μM of Sodium Stibogluconate (SS) and stimulated with 20 μg/ml $F(ab')_2$ anti-IgM. n=4 mice.

Capasso et al. supplementary Fig.6

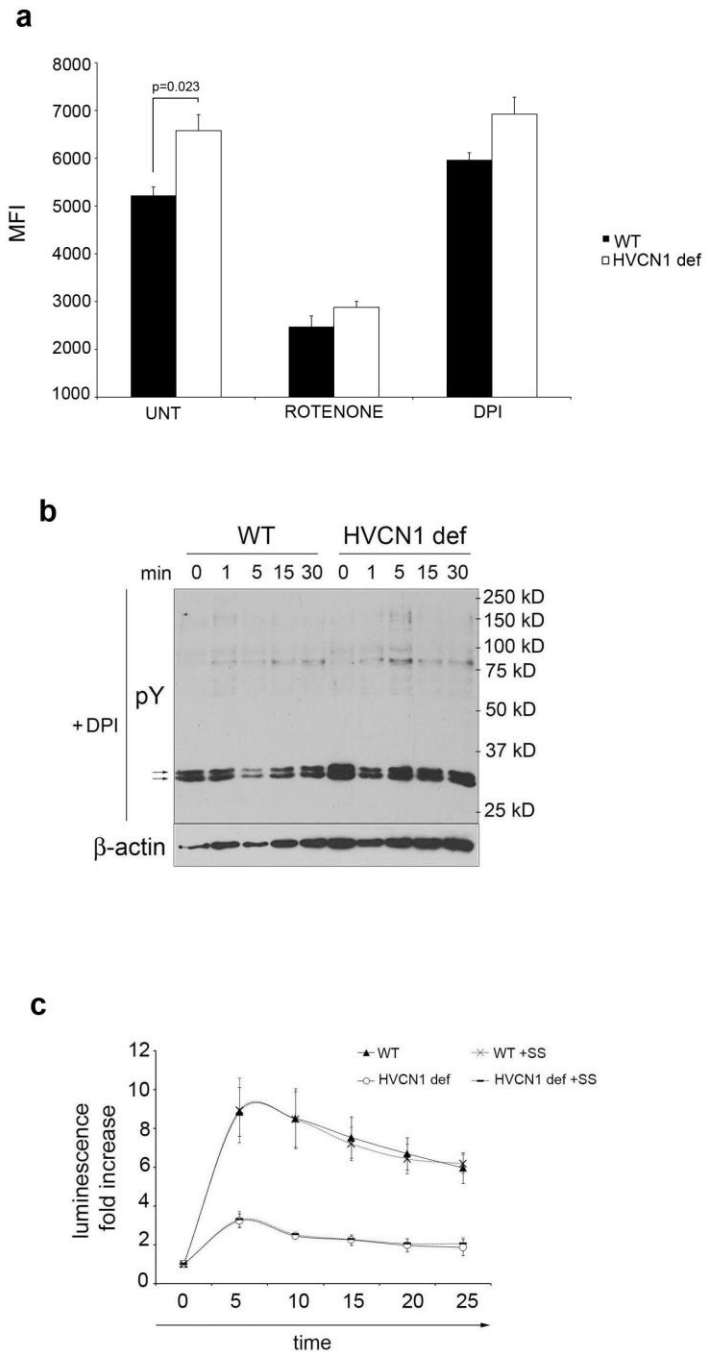

Supplementary Fig. 7

Endosomal pH and Ca^{++} mobilization in BCR-stimulated cells. Metabolic changes and Akt activation in LPS- and anti-CD40-stimulated B cells.

(a) pH measurements of internalized $F(ab')_2$ anti-IgM conjugated to a pH sensitive dye, pHrodo (Molecular Probes, Invitrogen), in wild-type and HVCN1-deficient splenic B cells. pHrodo will detect pH in internalized BCR-containing endosomes, any pHrodo-anti-IgM left on the surface will not emit any signal since the dye does not emit any fluorescence at neutral pHs. Cells were activated with 20 μg/ml $F(ab')_2$ anti-IgM-pHrodo and analyzed by flow cytometry at indicated times. An *in situ* standard curve was calculated resuspending cells in high K^+ buffers of known pH values in the presence of the H^+/K^+ antiporter nigericin, 4 hours after receptor internalization (not shown). Results indicate that absence of HVCN1 does not affect BCR-containing endomosal pH. n=3 mice.
(b) Ca^{++} mobilization in wild-type and HVCN1-deficient splenic B cells indicated as peak value (ratio at peak after stimulation minus value at steady state, n=7 mice).
(c) Analysis of metabolic rates in wild-type and HVCN1-deficient B cells after stimulation with 10 μg/ml LPS and 2 μg/ml anti-CD40 for 24h. Cells were cultured in a humidified incubator at 37°C for 24h before being analyzed on a Seahorse XF24 analyzer to measure mitochondrial respiration as oxygen consumption (OCR= oxygen consumption rate) and lactic acid production or glycolysis as extracellular acidification (ECAR= extracellular acidification rate). n=4 mice.
(d) Immunoblot analysis of phosphorylated Akt in wild-type and HVCN1-deficient splenic B cells activated with 10 μg/ml LPS and 2 μg/ml anti-CD40. Blots represent 3 independent experiments.
(e) ROS generation in wild-type and HVCN1-deficient B cells stimulated with 10 μg/ml LPS and 2 μg/ml anti-CD40. ROS production for wild-type cells stimulated with 20 μg/ml $F(ab')_2$ anti-IgM are reported for comparison. n= 4 mice.

Capasso et al. supplementary Fig. 7

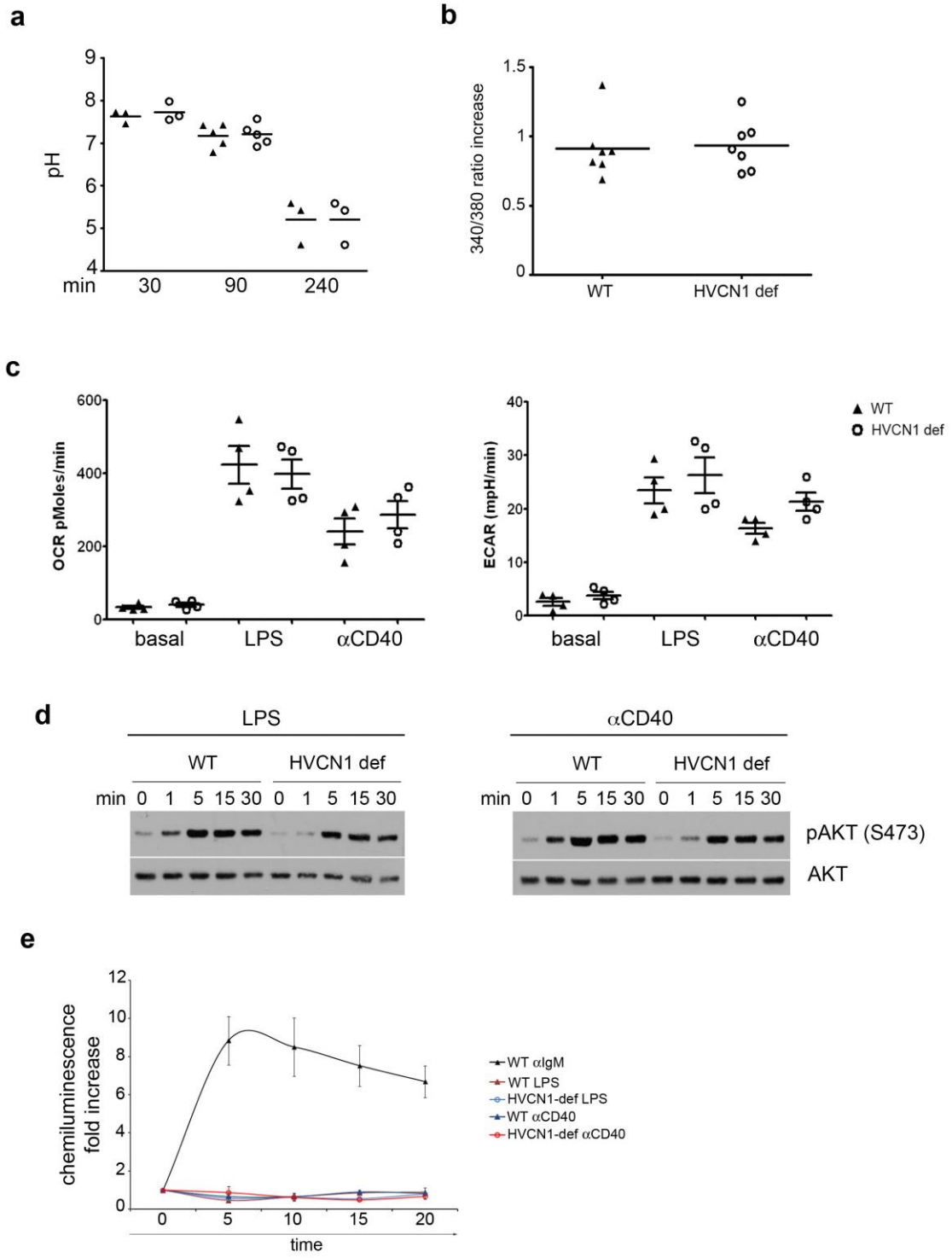

Supplementary Fig. 8

Wild-type and HVCN1-deficient B cell proliferation following LPS and anti-CD40 stimulation.

CFSE staining of splenic B cells stimulated with 10 μg/ml LPS (top panels) and 2μg/ml anti-CD40 for 72h. Similar results were obtained in 3 separate experiments.

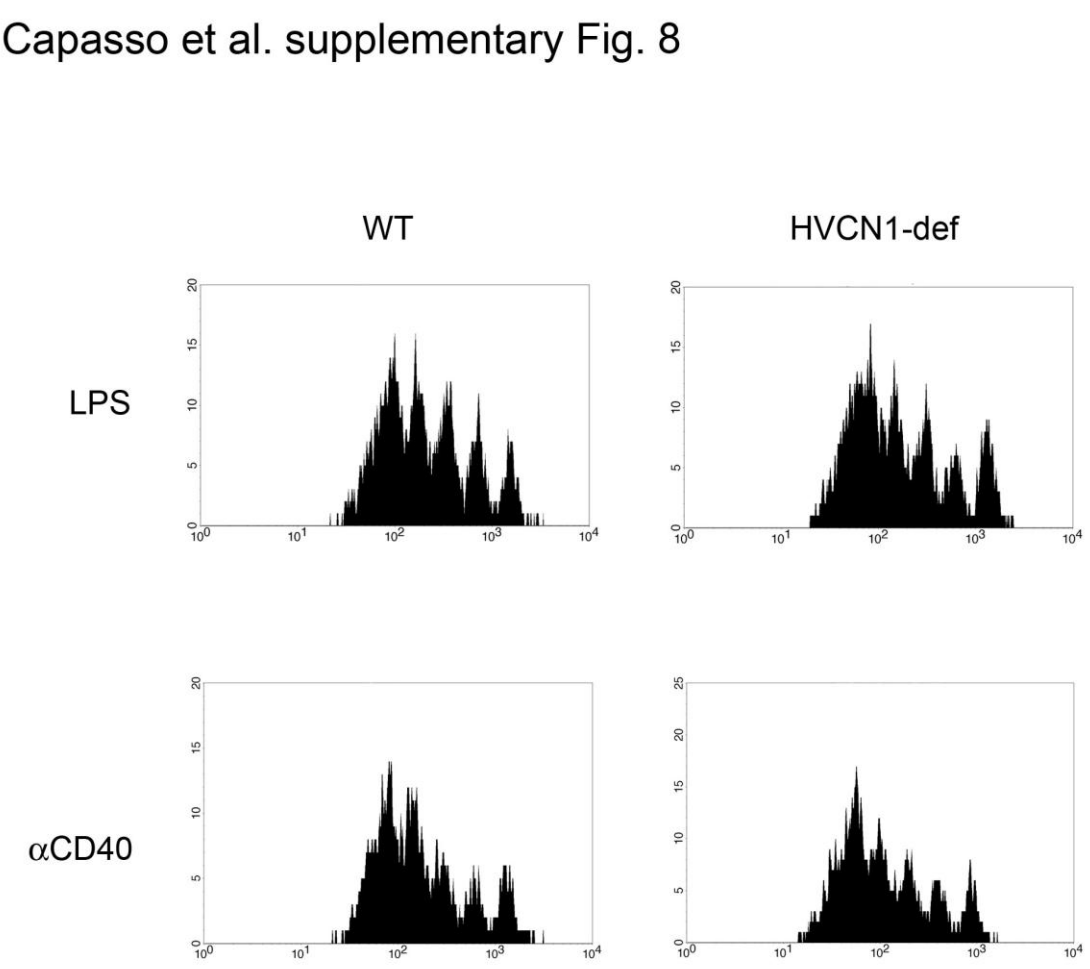

Supplementary Fig. 9

Schematic representation of HVCN1 role in the context of BCR stimulation.

Antigen binding to the BCR results in phosphorylation of ITAMs in the Igα/β heterodimer by LYN, creating docking sites for Syk[3]. This serves to amplify the BCR signaling by further recruitment and activation of Syk, which leads to PI3K activation, activation of Akt and increased glucose uptake and metabolism. Amplification of signaling is negatively regulated by CD22, which is also phosphorylated by LYN, providing a docking site for protein tyrosine phosphatase (PTP) SHP-1[28]. SHP-1 dephosphorylates Syk, counterbalancing ITAM-Syk mediated signal amplification. SHP-1 is inhibited by ROS, which oxidize a cysteine residue in the catalytic site of the enzyme[6]. BCR stimulation results in ROS generated by NADPH oxidase enzymatic complex[7-13,55], which transfers electrons across the plasma membrane/endosomes to molecules of oxygen. The transfer of one electron results in the production of $O^{\cdot}{}_2^-$ that combines with protons to form H_2O_2 and O_2 which freely diffuses through the membrane ($\mathbf{2O^{\cdot}{}_2^- + 2H^+ \rightarrow H_2O_2 + O_2}$)[56]. ROS generate a localized oxidizing environment causing inhibition of SHP-1, which results in amplification of BCR signal. HVCN1 sustains NADPH oxidase activity[18,19]. Therefore, in the absence of HVCN1, the oxidizing environment cannot be maintained and this results in SHP-1 remaining more active, reducing BCR-signal strength.

Capasso et al. supplementary Fig. 9

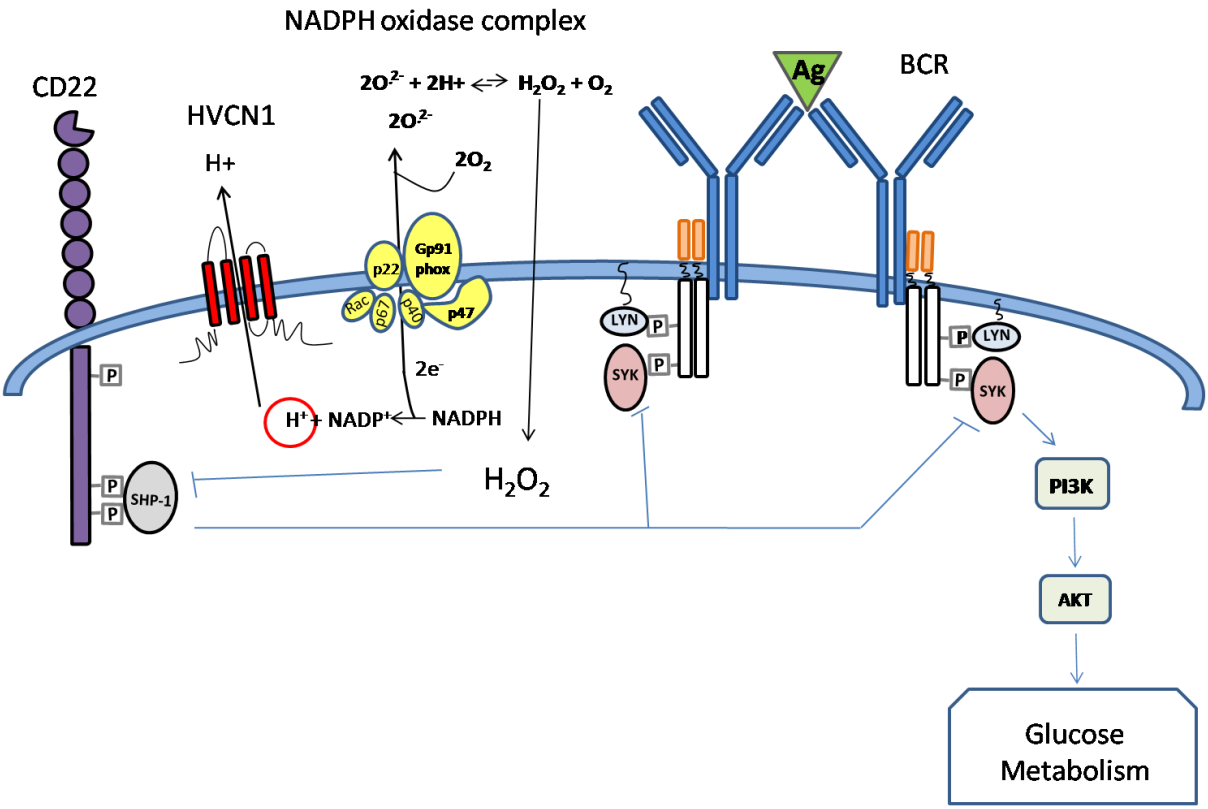

Supplementary Table 1.

HVCN1 associates with the B–cell receptor in BJAB cells.

HVCN1 was cloned into a pc3.1DNA vector, incorporating an N-terminal Strep-tag and transfected into BJAB cells to generate a stably strep-HVCN1 expressing D13 clone. In a) 100 x 10^6 empty vector (EV) control BJAB cells or D13 cells were lysed and strep-HVCN1 and associated proteins captured on streptactin beads for 1 h. at 4^{o}C. The beads were washed 4 times with buffer before eluting with SDS-PAGE sample buffer and separating on SDS-PAGE. Gel lanes were cut into 3 mm slices which were digested with trypsin and the eluted peptides analyzed by LC-MS/MS[21]. In b) stably expressing strep-HVCN1 cells were incubated with F(ab')$_2$ isotype control (non-stimulated) or 20 µg/ml (F(ab')$_2$ anti-IgM (stimulated) for 10 min. Cells were subsequently lysed and HVCN1 associated proteins identified by LC-MS/MS as described in a). The number of unique peptides identified and % coverage was determined by MUDPIT analysis and the table lists the number of peptides identified with MASCOT scores >35 and % percentage coverage of the protein sequence. Igβ and Ig kappa chain c region proteins were identified from one peptide (sequences shown in c), which were identified with >95% probability and high MASCOT scores.

a) HVCN1 associated proteins in stably expressing BJAB cells

	BJAB-EV		D13 Strep-HVCN1	
Protein	Peptides	Sequence coverage (%)	Peptides	Sequence coverage (%)
HVCN1	0	0	8	32
Ig mu chain C region	0	0	2	6
Ig kappa chain C region	0	0	0	0
CD22	0	0	3	5.5
Igβ	0	0	0	0
CD19	0	0	0	0

b) HVCN1 associated proteins before and after BCR stimulation

	ISOTYPE control		Anti-IgM	
Protein	Peptides	Sequence coverage (%)	Peptides	Sequence coverage (%)
HVCN1	6	28	8	32
Ig mu chain C region	4	12	7	19
Ig kappa chain C region	2	32	1	13
CD22	8	13	6	11
Igβ	0	0	1	5
CD19	0	0	6	20

c) Single peptide identification

Protein	Accession Number	Sample	Sequence	M/Z (Z=2)	Mascot score
Ig kappa chain C region	KAC_HUMAN	HVCN1 + Anti-IgM	(K)DSTYSLSSTLTLSK(A)	751.87	99
Igβ	Q53FS2_Human	HVCN1 + Anti-IgM	(R)VMGFSTLAQLK(Q)	605.87	65

Supplementary methods

Detection of pH in BCR-containing endosomes

pH of internalized BCR-containing endosomes was detected employing an $F(ab')_2$ anti-IgM conjugated to a pH sensitive dye, pHrodo (Molecular Probes, Invitrogen). The dye was conjugated to an $F(ab')_2$ anti-IgM according to manufactures instructions. pHrodo does not emit any fluorescence at neutral pH and emits a signal at 540 nm once the environment becomes more acidic. Fluorescence intensity is proportional to increase in acidification. After conjugation to an $F(ab')_2$ anti-IgM used to activate the cells, the dye will detect pH in internalized BCR-containing endosomes as these organelles become more acidic. Any antibody left on the surface will not emit any signal since the dye does not emit fluorescence at neutral pH. Cells were activated with 20 µg/ml of $F(ab')_2$ anti-IgM-pHrodo and analyzed by flow cytometry at indicated times. An *in situ* standard curve was calculated resuspending cells in high K^+ buffers of known pH values in the presence of the H^+/K^+ antiporter nigericin, 2 h after receptor internalization (not shown).

Plasmids and retroviral infection

Myc-tagged, HA-tagged, His-V5-tagged HVCN1 were cloned by PCR in pcDNA 3.1 vector (Invitrogen) or GFP-bicistronic MigR1 retroviral vector. Phoenix α packaging cell line was transfected with empty vector control and HVCN1 MigR1 plasmids by calcium phosphate transfection. Viral supernatants were collected after 24 h, 36 h and 48 h and frozen at –80°C until use. LK35.2 cells were infected by spinoculation at 450 x *g* for 90 min in the presence of 4 µg/ml polybrene (Sigma Aldrich), three times over a period of 2 days. At day 3, GFP^{hi} cells were sorted on a FacsVantage with CellQuest software (Becton Dickinson) and used for *in vitro* phosphorylation assays and patch clamp.

References for supplementary material

54. Suenaga, T. *et al.* Cloning of B cell-specific membrane tetraspanning molecule BTS possessing B cell proliferation-inhibitory function. *Eur. J. Immunol.* **37**, 3197–3207 (2007). cited in supplementary Fig. 1 legend.

55. Rodaway, A.R., Teahan, C.G., Casimir, C.M., Segal, A.W. & Bentley, D.L. Characterization of the 47-kilodalton autosomal chronic granulomatous disease protein: tissue-specific expression and transcriptional control by retinoic acid. *Mol. Cell. Biol.* **10**, 5388–5396 (1990). </jrn> this reference is cited in legend to supplementary Fig. 9

56. Decoursey, T.E. Voltage-gated proton channels and other proton transfer pathways. *Physiol. Rev.* **83**, 475–579 (2003).